The DOI for this manuscript is doi: 10.1175/JCLI-D-17-0793.1

Nearly synchronous multidecadal oscillations of surface air temperature in Punta Arenas and the Atlantic Multidecadal Oscillation index

Short title: Multidecadal oscillations of temperature in Punta Arenas

Mary Toshie Kayano Alberto W. Setzer

Instituto Nacional de Pesquisas Espaciais, Centro de Previsão de Tempo e Estudos Climáticos, São José dos Campos, SP, Brazil

Corresponding author: Mary T. Kayano

Email: mary.kayano@inpe.br

KEYWORDS: Climate variability, Teleconnection, South America, Atlantic Multidecadal Oscillation

Abstract

The Atlantic Multidecadal Oscillation (AMO) signature in southern South America (SA) is examined using Punta Arenas (53.0 °S; 70.85 °W) surface air temperature (T-air) during the 1888-2016 period. T-air shows multidecadal oscillations with a significant positive correlation of 0.77 to the AMO index. The relations of Punta Arenas T-air time series with the AMO-related global sea surface temperature (SST) and regional circulation anomaly patterns are discussed. During the warm (cold) AMO phase, a cold (warm) center in southwestern Atlantic waters induces low-level anticyclonic (cyclonic) anomalies in the region, which together with the cyclonic (anticyclonic) anomalies in the southeastern Pacific channel the northerly (southerly) flow over southern SA. This meridional flow transports warm (cold) air from lower (higher) latitudes into Punta Arenas region. Therefore, the temperature horizontal advection at low level is the main thermodynamic process that alters Punta Arenas T-air in a multidecadal time scale. The use of a relation between a long T-air surface sensor series in southern SA with the AMO presents a novel approach in climate monitoring and modelling.

1. Introduction

Rising in greenhouse gas concentrations drives the current global warming and the associated changes in the climate system (Houghton et al. 1990). Therefore, surface air temperature (T-air) is one of the most important climate variables, not only in this context, but also due to its natural variations. Nevertheless, reliable instrumental long T-air records are few and restricted to some regions in the globe. Consequently, detailed studies on the T-air variations have been hampered for many regions, including large regions of the South American continent, where reliable surface observations in a relatively dense network are available beginning mainly in the 1950s (Garreaud et al. 2009). Thus, the few studies found in the literature on T-air variations over South America (SA) examined mostly the interannual timescale variability or trends during the last decades. Studies on T-air long-term trends over SA, in general, used extreme temperatures and were restricted to regions such as the Brazilian Amazon (Victoria et al. 1998), Venezuela and Colombia (Quintana –Gomes 1999), Argentina (Rusticucci and Barrucand 2004) and southern Brazil (Marengo and Camargo 2008; Sansigolo and Kayano 2010). Vargas and Naumann (2008) suggested that secular trends identified in the minimum and maximum temperature time series in eight station in southern South America are driven by the set of wet days. Naumann and Vargas (2017) showed that these time series contain also oscillations with periods varying from 18 to 25 years. They also showed that these periodicities vary over time, in particular during the 1950-1970 decades when higher variability predominated. In the southern high-latitudes, Zazulie et al. (2010) analyzed T-air variations in the Antarctic South Orkney/Orcadas del Sur Island station (60.7 °S; 44.7 °W) and found no statistically significant trends from 1903 to 1950; however, for the remainder of the series a statistically significant warming was noticed throughout the four seasons of the year. Vincent et al. (2005) analyzed the trends in daily temperature extremes during the 1960-2000 period in eight countries of SA and found a consistent positive trend for the daily minimum temperature for stations located in its west and east coasts.

For the interannual time-scale, the El Niño-Southern Oscillation (ENSO) is the most important coupled ocean-atmosphere mode responsible for climate variations over SA (Ropelewki and Halpert 1987; 1989; Zhou and Lau 2001). This climate linkage occurs through alterations in the Walker and Hadley cells creating an atmospheric circulation bridge between the tropical Pacific and tropical SA, or through the anomalous large-scale Rossby wavetrain patterns that connect the tropical Pacific and extratropical SA (Zhou and Lau 2001). Due to the regional surface differences, the ENSO effects on the South American T-air present seasonal and regional dependences documented in previous studies. An El Niño (a La Niña) related abnormal warming (cooling) occurs in subtropical and southeastern SA during winter, in tropical SA during summer and autumn, and in northern and western tropical SA during spring (Kiladis and Diaz 1989; Halpert and Ropelewski 1992; Grimm 2003; 2004; Grimm et al. 2007; Grimm and Zilli 2009; Kayano et al. 2017).

The T-air variability over SA on timescales longer than the interannual has been analyzed in the context of the multidecadal variability in the Pacific Ocean (Dettinger et al. 2001; Collins et al. 2009; Kayano et al. 2017). Dettinger et al. (2001) found that the climate indices in the Pacific Ocean describing the decadal ENSO-like atmospheric-oceanic mode (Zhang et al. 1997) and Pacific Decadal Oscillation (PDO) (Mantua et al. 1997) are positively correlated with annual T-air over western tropical SA. For positive indices, they associated a warm tropical SA and a dry condition. In a similar analysis, Kayano et al. (2017) found seasonal differences of the non-ENSO T-air modes in SA. In their analysis, the first winter and first autumn modes show a warming in subtropical SA due to the warm advection; the first spring, the first summer, the second winter and the second autumn modes show a warming in the tropical SA and a cooling in subtropical SA, respectively associated with the dryness and wetness in these areas. Collins et al. (2009), using T-air at 2 m above the earth's surface from the National Centers for Environmental Prediction/ National Center for Atmospheric Research (NCEP/NCAR) reanalysis found warmer winters in tropical SA during the 1976-2007 period in relation to the 1948-75 period.

The above studies stressed the T-air variability in SA in the context of Pacific large-scale phenomena such as ENSO, PDO and ENSO-like decadal Pacific mode. In contrast, the signature of the Atlantic Multidecadal Oscillation (AMO) on the T-air variability in SA has received little attention. Nevertheless, some few studies using millennial temperature reconstructions provided indications on the existence of the AMO signature in southern SA. In fact, Villalba et al. (1996) found a main 72-year spectral peak in the second principal component of the factor analysis of the alerce tree-ring data for the 980-1974 period in northern Patagonia. They noted that this spectral peak is close to the 65 to 70-year oscillation in T-air registered in the North Atlantic by Schlesinger and Ramankutty (1994). Villalba et al. (1996) suggested a connection between T-air in northern Patagonia and North Atlantic through changes in the sea surface temperature (SST) in the Weddell Sea, which in turn occur as a response to multidecadal changes in the Atlantic thermohaline circulation shown in a modeling study by Crowley and Kim (1993). Nowadays, the T-air 65 to 70-year oscillation found by Schlesinger and Ramankutty (1994) is called the AMO, a natural oceanic variability, whose signature is noted in SST and is related to decadal to multidecadal changes in the thermohaline circulation (Kerr 2000; Delworth and Mann 2000; Knight et al. 2006).

In the present analysis, the relations of the AMO and the T-air variability in southern SA are examined using an instrumental T-air record at surface level. This study was firstly motivated by a multidecadal oscillation in annual Punta Arenas T-air time series noticed in an exploratory analysis. Punta Arenas (53.0 °S; 70.85 °W), Chile, is one of the surface stations in southern Patagonia, a region south of 51 °S in SA with similar T-air variations shown in a cluster analysis (Coronato and Bisigato 1998). This station has the longest reliable monthly T-air time series in southern SA, with few missing data, and spans from the end of the nineteen century up to the present (1888-2017). The availability of such a long period time series allow us to examine low-frequency oscillations in this station. Thus, the main objective of the present analysis is to investigate observational evidence on the multidecadal time scale oscillations in Punta Arenas T-air time series and its relation to the AMO.

Data and methodology used in the present analysis are described in the following section. The connections of Punta Arenas T-air multidecadal variations with the AMO-related SST and atmospheric circulation anomaly patterns are discussed in Section 3. Conclusions are drawn in Section 4.

2. Data and Methodology

Punta Arenas monthly T-air unadjusted (hereinafter referred to as PA_T-air) time series for the 1888-2016 period was obtained at https://data.giss.nasa.gov/gistemp/stdata/ (GISTEMP Team; Hansen et al. 2010). The 1888-2016 period with PA_T-air data availability defined it as the analysis period. We also used monthly gridded reanalyzed SST, sea level pressure (SLP), 1000 hPa and 850 hPa zonal and meridional winds and T-air. The SST data for the analysis period were obtained from the NOAA extended reconstructed SST version V4 (ERSST) data at a 2° by 2° latitude-longitude resolution grid available at www.esrl.noaa.gov/psd/data/gridded/data.noaa.ersst.v4.html (Huang et al. 2015). The COBE SST data provided by the NOAA/OAR/ESRL PSD, Boulder, Colorado, USA, from their Web site at https://www.esrl.noaa.gov/psd/ were also used (Ishii et al. 2005). The atmospheric circulation and thermodynamic data at a 1° by 1° latitude-longitude resolution grid for the 1888-2014 period were derived from the version V2C Twentieth Century Reanalysis (20CR) Project available at www.esrl.noaa.gov/psd/data/gridded/data.20thC_ReanV2c.html (Compo et al. 2011). Temperature horizontal advection at 850 hPa was calculated in each grid point for the 1888-2014 period. The COBE SST data were used to test the robustness of the correlation map between PA_T-air and the SST anomalies. SST data were used for the other analyses involving the ERSST.

The revised AMO index was calculated using the SST time series in the North Atlantic region limited at the equator, 70 °N, 80 °W and the Greenwich longitude and the global SST in the band between 70 °N and 70 °S. This index is defined as the de-trended SST anomalies averaged in the North Atlantic region from which the global SST averaged anomalies are removed (Trenberth and Shea 2006). This index was smoothed with a 121-month running mean filter. The monthly SST anomalies were obtained as the departures from means of the 1888-2016 period.

Because the long-term trends are not of interest here, the linear trends in the anomaly time series were removed by subtracting the linear least-squares trends. So, monthly de-trended SST, SLP, 1000 hPa zonal and meridional winds and T-air, and 850 hPa temperature horizontal advection anomalies were calculated in each grid point. Prior to calculating the monthly de-trended PA_T-air anomaly time series, its missing values were linearly interpolated. The climatologies and the linear trends were based on the

1888-2016 period for the PA_T-air and SST, and on the 1888-2014 period for the SLP, 1000 hPa zonal and meridional winds and T-air, and 850 hPa temperature horizontal advection.

The Morlet wavelet analysis was used to perform a spectrum analysis of the de-trended PA_T-air anomaly time series, after Torrence and Compo's (1998) procedure.

As for the AMO definition, the 121-month running mean was the filter used for the PA_T-air and the reanalyzed variables. The relation between the filtered PA_T-air and AMO index time series was obtained through the linear simultaneous correlation calculation. Also, linear simultaneous correlation maps between filtered PA_T-air and the other filtered variables (SLP, 1000 hPa winds, 850 hPa temperature horizontal advection) were constructed. In order to assess the statistical significance of the correlations, the Ebisuzaki (1997) test with 1,000 pairs of Fourier series with random phases of the filtered PA_T-air time series and of the other involved time series was used. The significance was obtained in a manner similar to the bootstrap method. In the case of the correlation maps, it is common practice that absolute correlations greater than 0.6 are significant at the 90% confidence level.

Annual average PA_T-air values for the 1888-2016 period were used to identify the cold and warm years in Punta Arenas. These values, ranked from 1 for the smallest value to 129 for the largest value, provided the percentile rank (R) time series varying from approximately zero to 1. The lower (20%) and upper (80%) quintiles were used to classify cold and warm years in Punta Arenas, respectively. These years were stratified in the AMO phases and are listed in Table 1. Anomaly composites of the unfiltered 1000 hPa T-air, SLP and low-level wind anomalies of the cold years during the cold AMO phase, and of the warm events during the warm AMO phase were calculated. The statistical significance of the composites was assessed using the Student-t test and considering the number of years in the composite as degrees of freedom. For a variable X with n values and S standard deviation showing a Student-t distribution, only the means with absolute values exceeding $t_{\propto,(n-1)}S/\sqrt{(n-1)}$ are statistically significant (Panofsky and Brier 1968). The confidence level of 90% was used in all composites.

3. Results

3.1. Punta Arenas T-air and AMO index

The Global Wavelet Power (GWP) of PA_T-air time series shows a main 80-year peak, and two secondary peaks, one at 8 years and another one at 28 years (Figure 1b). All three peaks are significant at a 5% level. The 8-year peak in the GWP is due to the significant variances observed during the 1888-1920 period; and the 28-year peak is due to the significant variances during the 1888-1940 and 1970-2000 periods, and the main 80-year peak is due to the significant variances during the entire period of analysis (Figure 1a). For this latter peak, the significant variances are within the cone of influence, the region where the edge effects are important (Torrence and Compo 1998), and an option is to disregard this peak. However, Villalba et al. (1996) found a main 72-year spectral peak in the second principal component of the factor analysis of the alerce tree-ring T-air data for the 980-1974 period in northern Patagonia. Although their analysis was based on locations north of Punta Arenas, the similar magnitude of the peaks give us more confidence on the existence of a multidecadal signal in PA_T-air time series.

This multidecadal signal in PA_T-air is also present when comparing the filtered PA_T-air and AMO index time series. These time series show nearly synchronous highly correlated multidecadal fluctuations with a linear simultaneous correlation of 0.77, which is statistically significant at 98% confidence level (Figure 2). The statistical significance of this correlation was tested using the Ebisuzaki (1997) method, in which 1000 pairs of Fourier series with random phases of the filtered AMO and PA_T-air time series were obtained. The positive correlation means that Punta Arenas is anomalously warm (cold) during the warm (cold) AMO phase. This is an unexpected result by the fact that Punta Arenas is some 13,000 km away from the North Atlantic, where the largest AMO-related SST anomalies are centered. Figure 2 shows that the warm (or positive) AMO phase occurred during the 1888-1898, 1930-1960 and 1995-2016 periods and the cold (or negative) one, during the 1901-1926 and 1934-1964 periods.

In order to examine the AMO related global SST anomaly patterns, the maps of the unfiltered SST anomalies averaged during the warm and cold AMO phases were obtained (Figure 3). These maps show nearly reversed sign patterns and reproduce the AMO-related SST antisymmetric anomaly pattern between the North and South Atlantic sectors, previously obtained using distinct methods and areas of analysis from those used here (Enfield and Mestas-Nuñez 1999; Mestas-Nuñez and Enfield 1999; Goldenberg et al. 2001; Latif et al. 2006; Deser et al. 2010). An interesting feature is the presence of negative (positive) SST anomalies surrounding most of southern SA during warm (cold) AMO phase. This result strongly suggests that the positive relation between PA_T-air and the AMO index can not be justified by the dominant low-level westerlies over southern SA and this aspect is further examined in the following sub-section.

3.2 Multidecadal relations between Punta Arenas T-air and oceanic and atmospheric conditions

Coherently with the positive correlation between the PA_T-air and AMO index time series, the correlation map for the ERSST SST shows the significant positive correlations in the Atlantic Ocean north of 5 °S, and the negative ones in the extratropical South Atlantic centered approximately at 60 °S, 30 °W and in the southeastern Pacific (Figure 4a). The correlation map for the COBE SST presents a similar pattern, except for less significant negative correlations in the extratropical South Atlantic and southeastern Pacific (Figure 4b). The correlation pattern reproduces the main features noted during the warm AMO phase (Figures 3 and 4a). This result is consistent with the maps of the observed surface temperature regressed onto the AMO index previously obtained (Figure 2 by Ting et al. 2011; Figure 1 by Lyu and Yu 2017). Both analyses show positive anomalies over the Punta Arenas area and the positive correlations between PA_T-air and the SST anomalies in the North Atlantic here found are consistent with previous findings.

In this context the anomalously warm (cold) condition in Punta Arenas is associated with anomalously cold (warm) surface waters in southwest Atlantic and southeastern Pacific. However, this association can not be explained by the dominant low-level westerlies over southeastern Pacific and southern SA that occur throughout the year (Prohaska 1976; Barros et al. 2002). This westerly flow over an underlying cold (warm) region in the southeastern Pacific would bring cold (warm) condition into southern SA.

In fact, a low-level circulation pattern with a strong meridional component over southern SA replaces the low-level westerlies, as shown in the correlation map between PA_T-air and SLP and 1000 hPa winds (Figure 5b). The interpretation is that the low-level northerly (southern) flow channels the lower (higher) latitude warm (cold) air into southern SA. This flow is part of the strong anticyclonic (cyclonic) anomalies associated with an anomalous high (low) pressure center in southwestern Atlantic and relatively weak opposite circulation and SLP anomaly patterns in southeastern Pacific (Figures 5a and 5b). The anomalous high (low) pressure center is consistent with cold (warm) surface waters in southwestern Atlantic during the warm (cold) AMO phase (Figures 4 and 5a). Concordantly, the correlation map between filtered PA_T-air and 850 hPa temperature horizontal advection shows positive correlations in eastern southern SA (Figure 6). Therefore, the warm (cold) advection from the lower (higher) latitudes is the main process that alters PA_T-air in a multidecadal time scale.

3.3 Composite analyses

Table 1 shows the years in lower (20%) and upper (80%) quintiles of PA_T-air, which were stratified in the AMO phases. Out of 22 years in the lower quintile, 20 occurred during the cold AMO phase. This means that 91% of the cold years in Punta Arenas occurred during the cold AMO phase. Furthermore, some of these years occurred sequentially, as for the cold period of 1905-1909 and 1969-1974, what indicates the low-frequency modulation of the PA_T-air variations. Concerning the upper quintile, 12 out of 25 occurred during the warm AMO phase. This result indicates no predominance of the warm Punta Arenas years in relation to the AMO phases. This apparent inconsistent result is due to the occurrence of warm years during the cold AMO phase from 1893 to 1923 (Figure 7). However, there is a predominance of warm years after 1923 during warm AMO phase. Recalling that the quintile analysis was based on the PA_T-air data without any filtering process, the coherency of the upper and lower quintiles with the warm and cold AMO phases gives us more confidence on the results from the correlation analysis for filtered data.

In order to illustrate the coherency of the above results, composite analyses were done using unfiltered data for two cases: warm Punta Arenas during the warm AMO phase and cold Punta Arenas during the cold AMO phase. Most characteristics of the SST anomaly pattern noted during the warm (cold) AMO phase are reproduced for the warm (cold) Punta Arenas composite of 1000 hPa T-air (Figures 3a, 3b, 8a and 9a). Also, the positive (negative) 1000 hPa T-air anomalies found over Punta Arenas and the north of the Antarctic Peninsula for the warm (cold) composite confirm Lyu and Yu (2017) findings for Punta Arenas. Consistent with the above analyses, for the warm (cold) Punta Arenas composite, the low-level wind anomaly patterns show anticyclonic (cyclonic) anomalies in the southwestern Atlantic and opposite sign circulation anomalies in the southeastern Pacific (Figures 8b and 9b).

4. Discussion and conclusions

Using an instrumental surface air temperature (T-air) record in Punta Arenas (53.0 °S; 70.85 °W), PA_T-air, for the 1888-2016 period, the AMO signature in South America (SA) T-air is examined. It is worth recalling that we de-trended the data by removing the linear least-squares trend in each time series, and thus the anthropic effects are not considered in the present analysis.

PA_T-air shows multidecadal oscillations which are simultaneously highly and positively correlated with the Atlantic Multidecadal Oscillation (AMO) index. This positive correlation is an unexpected result because Punta Arenas is 13,000 km away from the North Atlantic, where the AMO signature is strong (Figure 3) (Enfield et al. 2001; Goldenberg et al. 2001; Latif et al. 2006; Deser et al. 2010). PA_T-air time series shows a main 80-year spectral peak that agrees with Villalba et al. (1996) findings using the alerce tree-ring T-air data for the 980-1974 period in northern Patagonia; they found a main 72-year spectral peak in the second principal component of the factor analysis of these data.

This highly significant simultaneous correlation between PA_T-air and AMO index does not imply a causal relation and means that both time series may reflect the same phenomenon. Here we examined this relation and provided observational evidence that it occurs through changes in the regional low-level circulation modulated by the AMO. The AMO-related near global sea surface temperature (SST) anomaly pattern previously found (Enfield and Mestas-Nuñez 1999; Mestas-Nuñez and Enfield 1999; Deser et al. 2010) were reproduced using the 1888-2016 data. A meridional SST anomaly pattern with positive (negative) values in the North Atlantic and opposite sign anomalies in the extratropical South Atlantic is established during the warm (cold) AMO phase (Figure 4). The anomalously cold (warm) center induces low-level anticyclonic (cyclonic) anomalies associated with an anomalously high (low) pressure system in the southwestern Atlantic (Figure 5). This center, together with the low-level cyclonic (anticyclonic) anomalies in the southeastern Pacific channels the low-level northerly (southerly) flow over southern SA, so that warm (cold) air is advected from the lower (higher) latitudes into Punta Arenas region (Figures 5 and 6). Therefore, the low-level westerlies that blow throughout the year and influence the climate in this region (Prohaska 1976; Barros et al. 2002) are weakened due to a multidecadal low-level circulation background with a dominant meridional component. Thus, the temperature horizontal advection from the lower (higher) latitudes is the main thermodynamic process that alters PA_T-air in a multidecadal time scale. Punta Arenas is one of the surface stations in southern Patagonia, a region south of 51 °S in SA with similar T-air variations shown in a cluster analysis (Coronato and Bisigato 1998). So, it is likely that the results for Punta Arenas might be extended for other stations in southern SA.

The analysis here showed that an unambiguous relation between PA_T-air and the AMO occurs throughout the associated atmospheric circulation changes in the southern SA region and surrounding oceanic areas. This result strongly suggests that other local atmospheric systems, such as the South American low-level jet, the South Atlantic Convergence zone, the Antarctic Oscillation as well as the South Atlantic variability modes might also be modulated to some extent by the AMO. These aspects are out of the scope of the present analysis and will be analyzed in future studies. We acknowledge that uncertainties might exist in the reconstructed SST data and in the reanalyzed atmospheric (20CR) data used here. We tested the sensitivity of the results to the period used by recalculating the SST and 1000 hPa wind composites considering the events before and after 1950 separately. The main SST and wind anomaly patterns for the total period were reproduced for both periods (before and after 1950). In the case of cold Punta Arenas during cold AMO phase, the patterns for the period after 1950 represent better the corresponding patterns of the total period. In contrast, for the case of warm Punta Arenas during the warm AMO phase, the patterns for the period before 1950 represent better the corresponding patterns of the total period. The weaker representation of the cold (warm) Punta Arenas during cold (warm) AMO phase patterns during the period before (after) 1950 is due to the smaller number of events than during the complementary period. Therefore, the number of the events in the composites is more crucial than the period of the analysis in defining the variable patterns. This test indicated that the uncertainties at the beginning of the time series did not affect our results and thus it guarantees the robustness of our results.

As far as we know, the relations of the T-air variations in southern SA registered in an instrumental time series and the AMO have not been discussed before. Our knowledge about these relations might be useful for climate monitoring purposes.

Furthermore, the results here reinforce that climate modelling studies should pay attention to the regional variations of the AMO-related variability.

5. Acknowledgements

The authors thank the two anonymous reviewers for their helpful comments and suggestions. The first author was partially supported by the Conselho Nacional de Desenvolvimento Científico e Tecnológico (CNPq) of Brazil under grant 302322/2017-5.

References

Barros, V. R., A. M. Grimm, and M. E. Doyle, 2002: Relationship between temperature and circulation in southeastern South America and its influence from El Niño and La Niña events. *J. Meteor. Soc. Japan*, **80**, 21-32.

Collins, J. M., R. R. Chaves, and V. S. Marques, 2009: Temperature Variability over South America. *J. Climate*, **2**, 5854-5869.

Compo, G. P., and Coauthors, 2011: The Twentieth Century Reanalysis Project. *Quart. J. Roy. Meteor. Soc.*, **137**, 1-28. doi: 10.1002/qj.776.

Coronato, F., and A. Bisigato, 1998: A temperature pattern classification in Patagonia. *Int. J. Climatol.*, **18**, 765-773.

Crosby, D.S., L.C. Breaker, and W.H. Gemmill, 1993: A proposed definition for vector correlation in geophysics: Theory and application. *J. Amos. Oceanic Tech.*, **10**, 355-367.

Crowley, T. L., and K.-Y. Kim, 1993: Towards development of a strategy for determining the origins of decadal-centennial scale climate variability. *Quart. Sci. Rev*., **12**, 375-385.

Delworth, T. L., and M. E. Mann, 2000: Observed and simulated multidecadal variability in the Northern Hemisphere. *Climate Dyn.*, **16**, 661–676.

Deser, C., M. A. Alexander, S.-P. Xie, and A. S. Phillips, 2010: Sea surface temperature variability: patterns and mechanisms. *Ann. Rev. Marine Sci*., **2**, 115-143.

Dettinger, M. D., D. S. Battisti, R. D. Garreaud, G. J. McCabe, and C. M. Bitz, 2001: Interhemispheric effects of interannual and decadal ENSO-like climate variations on the Americas. *Interhemispheric climate linkages: Present and Past Climates in the Americas and their Societal Effects*, V. Markgraf, Ed., Academic Press, Massachusetts, 1-16.

Ebisuzaki, W., 1997: A method to estimate the statistical significance of a correlation when the data are serially correlated. *J. Climate*, **10**, 2147-2153.

Enfield, D. B., and A. Mestas-Nuñez, 1999: Multiscale variabilities in global sea surface temperatures and their relationships with tropospheric climate patterns. *J. Climate* **12**, 2719-2733.

Enfield, D. B., A. M. Mestas-Nuñez, and P. J. Trimple, 2001: The Atlantic multidecadal oscillations and its relation to rainfall and river flows in the continental U.S. *Geophys. Res. Lett.*, **28**, 2077–2080, doi: 10.1029/2000GL012745.

Garreaud, R. D., M. Vuille, R. Compagnucci, and J. Marengo, 2009: Present-day South American climate. *Palaeogeog., Palaeoclimatol., Palaeoecol.*, **281**, 180-195, doi: 10.1016/j.palaeo.2007.10.032.

Goldenberg, S. B, C. Landsea, A. M. Mestas-Nuñez, and W. M. Gray, 2001: The recent increase in Atlantic hurricane activity: causes and implications. *Science*, **293**, 474–479, doi: 10.1126/science.1060040.

Grimm, A. M., 2003: The El Niño impact on the summer monsoon in Brazil: regional processes versus remote influences. *J. Climate,* **16**, 263-280.

Grimm, A. M., 2004: How do La Niña events disturb the summer monsoon system in Brazil? *Climate Dyn.*, **22**, 123-138.

Grimm, A. M., J. Pal, and F. Giorgi, 2007: Connection between spring conditions and peak summer monsoon rainfall in South America: Role of soil moisture, surface temperature, and topography in eastern Brazil. *J. Climate,* **20**, 5929–5945.

Grimm, A. M., and M. T. Zilli, 2009: Interannual variability and seasonal evolution of summer monsoon rainfall in South America. *J. Climate*, **22**, 2257-2275.

GISTEMP Team. 2017: *GISS Surface Temperature Analysis (GISTEMP)*. NASA Goddard Institute for Space Studies. Dataset accessed 2017-08-15 at https://data.giss.nasa.gov/gistemp/.

Halpert, M. S., and C. F. Ropelewski, 1992: Surface temperature patterns associated with the Southern Oscillation. *J. Climate,* **5**, 577-593.

Hansen, J., R. Ruedy, M. Sato, and K. Lo, 2010: Global surface temperature change, *Rev. Geophys.*, **48**, RG4004, doi:10.1029/2010RG000345.

Huang, B., and Coauthors, 2015: Extended reconstructed sea surface temperature version 4 (ERSST.v4). Part I: Upgrades and intercomparisons. *J. Climate*, **28**: 911–930. doi:10.1175/JCLI-D-14-00006.1

Houghton, J.T., G.J. Jenkins and J.J. Ephraums (eds.), 1990: Climate Change: The IPCC Scientific Assessment. Report prepared for Intergovernmental Panel on Climate

Change by Working Group I. Cambridge University Press, Cambridge, Great Britain, New York, NY, USA and Melbourne, Australia 410 pp.

Ishii, M., A. Shouji, S. Sugimoto, and T. Matsumoto, 2005: Objective analyses of sea-surface temperature and marine meteorological variables for the 20th Century using ICOADS and the Kobe Collection. *Int. J. Climatol.*, **25**, 865-879.

Kayano, M. T., R. V. Andreoli, R. A. F. Souza, and S. R. Garcia, 2017: Spatio-temporal variability modes of surface air temperature in South America during 1951-2010: ENSO and non-ENSO components. *Int. J. Climatol., (published online).*

Kerr, R. A., 2000: A North Atlantic climate pacemaker for the centuries. *Science,* **288**, 1984–1986, doi: 10.1126/science.288.5473.1984.

Kiladis, G., and H. F. Diaz, 1989. Global climatic anomalies associated with extremes in the Southern Oscillation. *J. Climate,* **2**, 1069-1090.

Knight, J. R., C. K. Folland, and A. A. Scaife 2006: Climate impacts of the Atlantic multidecadal oscillation. *Geophys. Res. Lett.*, **33,** L17706, doi: 10.1029/2006GL026242.

Latif, M., M. Collins, H. Pohlmann, and N. Keenlyside, 2006: A review of predictability studies of Atlantic sector climate on decadal time scales. *J. Climate*, **19**, 5971-5987.

Lyu, K., and J.-Y. Yu, 2017: Climate impacts of the Atlantic Multidecadal Oscillation simulated in the CMIP5 models: A re-evaluation based on a revised index. *Geophys. Res. Lett*., **44**, 3867-3876, doi:10.1002/2017GL072681.

Mantua, N. J., S. R. Hare, Y. Zhang, J. M. Wallace, and R. C. Francis, 1997: A Pacific interdecadal climate oscillation with impacts on salmon production. *Bull. Amer. Meteor. Soc.,* **78**, 1069-1079.

Marengo, J. A., and C. C. Camargo, 2008: Surface air temperature trends in southern Brazil for 1960–2002. *Int. J. Climatol*., **28**, 893–904.

Mestas-Nuñez, A. M., and D. B. Enfield, 1999: Rotated global modes of non-ENSO sea surface temperature variability. *J. Climate,* **12**, 2734–2746.

Naumann, G., and W. Vargas, 2017: Variabilidad de baja frecuencia de la persistencia de la temperatura en el sudeste de Sudamérica. *Rev. Bras. Meteor*., **32**, 1-12.

Panofsky, H. A., and G. W. Brier, 1968: *Some applications of statistics to Meteorology*, Pennsylvania State University, Pennsylvania, 224p.

Prohaska, F. J., 1976: Climates of Central and South America. *World Survey of Climatology* (vol. 12). W. Schwerdtfeger, Ed., Elsevier, Amsterdam, 532 pp.

Quintana-Gomez, R., 1999: Trends of maximum and minimum temperature in northern South America. *J. Climate*, **12**, 2104–2112.

Ropelewski, C. F., and M. S. Halpert, 1987: Global and regional scale precipitation patterns associated with the El Niño/Southern Oscillation. *Mon. Wea. Rev.,* **115**, 1606-1626.

Ropelewski, C. F., and M. S. Halpert, 1989: Precipitation patterns associated with the high index phase of the Southern Oscillation. *J. Climate,* **2**, 268-284.

Rusticucci, M., and M. Barrucand, 2004: Observed trends and changes in temperature extremes over Argentina. *J. Climate,* **17**, 4099–4107.

Sansigolo, C. A., and M. T. Kayano, 2010: Trends of seasonal maximum and minimum temperatures and precipitation in southern Brazil for the 1913-2006 period. *Theor. Appl. Climatol.,* **101**, 209-216, doi: 10.1007/s00704-010-0270-2.

Schlesinger, M. E., and N. Ramankutty, 1994: An oscillation in the global climate system of period 65–70 years. *Nature,* **367**, 723–726.

Ting, M., Y. Kushnir, R. Seager, and C. Li, 2011: Robust features of Atlantic multi-decadal variability and its climate impacts. *Geophys. Res. Lett*., **38**, L17705, doi:10.1029/2011GL048712.

Torrence, C., and G. P. Compo 1998: A practical guide to wavelet analysis. *Bull. Amer. Meteor. Soc.*, **79**, 61-78.

Trenberth, K. E., and D. J. Shea, 2006: Atlantic hurricanes and natural variability in 2005. *Geophys. Res. Lett*., **33**, L12704, doi: 10.1029/2006GL026894.

Vargas, W.M., and G. Naumann, 2008: Impacts of climatic change and low frequency variability in reference series on daily maximum and minimum temperature in southern South America. *Reg. Environ. Change*, **8**, 45–57, doi: 10.1007/s10113-007-0041-5.

Victoria, R. L., L. A. Martinelli, J. M. Moraes, M. V. Ballester, and A. V. Krushche, 1998: Surface air temperature variations in the Amazon region and its borders during this century. *J. Climate*, **11**, 1105–1110.

Villalba, R., J. A. Boninsegna, A. Lara, T. T. Veblen, F. A. Roig, J. C. Aravena, and A. Ripalta 1996: Interdecadal climatic variations in millennial temperature reconstructions from southern South America. *Climatic Variations and Forcing Mechanisms of the last 2000 years*. P. D. Jones, R. S. Bradley, and J. Jousel, Eds., NATO ASI Series (vol. 41), Springer-Verlag, Berlin Heidelberg, 161-189.

Vincent, L. A., and Coauthors, 2005: Observed trends in indices of daily temperature extremes in South America 1960–2000. *J. Climate*, **18**, 5011–5023.

Zazulie, N., M. Rusticucci, and S. Solomon, 2010: Changes in climate at high southern latitudes: A unique daily record at Orcadas spanning 1903–2008. *J. Climate*, **23**, 189-196, doi: 10.1175/2009JCLI3074.1

Zhang, Y., J. M. Wallace, and D. S. Battisti, 1997: ENSO-like interdecadal variability. *J. Climate*, **10**, 1004–1020.

Zhou, J., and K. M. Lau, 2001: Principal modes of interannual and decadal variability of summer rainfall over South America. *Int. J. Climatol.* **21**, 1623-1644.

Figure Captions

Figure 1 – (a) Local wavelet power spectrum of the continuous wavelet transform of PA_T-air normalized by $1/\sigma^2$ (σ^2=1°C^2); b) Global Wavelet Power (GWP) (in variance units). The shaded contours in (a) are at normalized variances varying from 5 to 40 with interval of 5. The closed contours in (a) encompass significant variances at 95% confidence level and the region where the edge effects are important is under the U-shape curve in (a). The dashed curve in (b) is the significance at 5% level assuming a red-noise spectrum.

Figure 2 – Monthly filtered PA_T-air anomaly (black line) and AMO index (red line) time series. Both filtered with a 121-month running mean filter for the 1893-2011 period. The unit is °C.

Figure 3 – SST anomalies averaged during: a) warm AMO phase; b) cold AMO phase. The unit is °C. Areas with dotted shades encompass significant values. The continuous (dashed) line encompasses positive (negative) significant anomalies at the 95% confidence level using the Student-t test for mean. The purple dot in both maps gives the location of Punta Arenas.

Figure 4 – Correlations between filtered PA_T-air and filtered SST using: a) ERSST data; b) COBE data. Areas with dotted shades encompass significant values. The continuous (dashed) line encompasses positive (negative) significant values at the 90% confidence level using the Ebisuzaki (1997) test for correlation. The purple dot in both maps illustrates the location of Punta Arenas.

Figure 5 – Correlations between filtered PA_T-air and filtered: a) SLP; b) 1000 hPa winds. In a), the continuous (dashed) line encompasses positive (negative) significant values at the 90% confidence level using the Ebisuzaki (1997) test for correlation.

In b), shaded areas encompass significant vector correlation at the 90% confidence level using the Crosby et al. (1993) test for vector correlation. Arrow at the bottom illustrates the base magnitude of the correlation vector. The purple dot in both maps illustrates the location of Punta Arenas.

Figure 6– Correlations between filtered PA_T-air and filtered 850 hPa temperature horizontal advection. Display is the same as in Figure 5a.

Figure 7 - Temporal occurrence of upper (blue) and lower (red) quintiles of the PA_T-air indicated, respectively by 1 and -1 and the AMO index (°C) multiplied by 3 (black continuous line).

Figure 8 – a) Composites for warm Punta Arenas during the warm AMO phase of: a) 1000 hPa T-air anomalies; b) 1000 hPa wind anomalies. In a), areas with dotted shades encompass significant values and the continuous (dashed) lines encompass positive (negative) significant values. In b), shaded areas encompass significant wind vectors. The Student-t test for mean at the 95% confidence level was used. Arrow at the bottom illustrates the base magnitude of the wind vector. The units are °C for 1000 hPa T-air, and ms^{-1} for wind vector.

Figure 9 – a) Composites for cold Punta Arenas during the cold AMO phase of: a) 1000 hPa T-air anomalies; b) 1000 hPa wind anomalies. Display is the same as in Figure 8.

Table captions

Table 1. Cold and warm years in Punta Arenas stratified according to the AMO phases.

Table 1. Cold and warm years in Punta Arenas stratified according to the AMO phases.

Cold Punta Arenas during cold AMO phase	Warm Punta Arenas during warm AMO phase	Cold Punta Arenas during warm AMO phase	Warm Punta Arenas during cold AMO phase
1905, 1906, 1907, 1908, 1909, 1914, 1966, 1969, 1970, 1971, 1972, 1973, 1974, 1976, 1977, 1984, 1986, 1991, 1995	1931, 1936, 1938, 1941, 1942, 1943, 1944, 1945, 1952, 1956, 1962, 2004, 2016	2000, 2002	1893, 1894, 1895, 1896, 1901, 1904, 1912, 1916, 1917, 1919, 1920, 1921, 1922

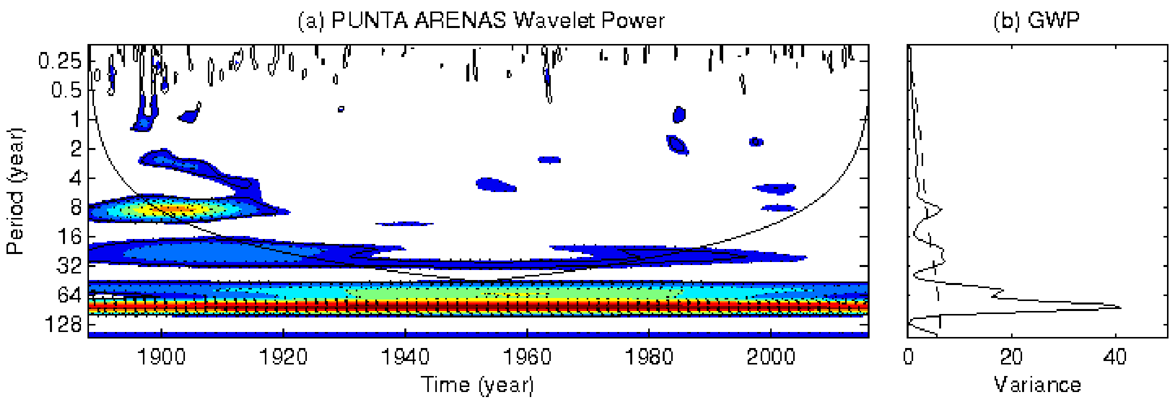

Figure 1 – (a) Local wavelet power spectrum of the continuous wavelet transform of PA_T-air normalized by $1/\sigma^2$ (σ^2=1°C^2); b) Global Wavelet Power (GWP) (in variance units). The shaded contours in (a) are at normalized variances varying from 5 to 40 with interval of 5. The closed contours in (a) encompass significant variances at 95% confidence level and the region where the edge effects are important is under the U-shape curve in (a). The dashed curve in (b) is the significance at 5% level assuming a red-noise spectrum.

Figure 2 Click here to download Rendered Figure Figure 2vf1.docx

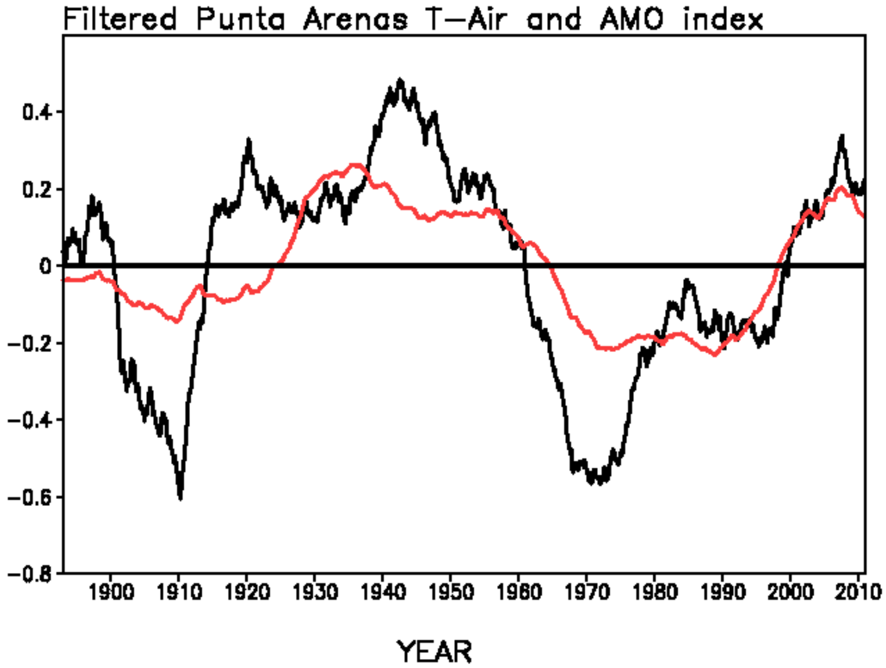

Figure 2 – Monthly filtered PA_T-air anomaly (black line) and AMO index (red line) time series. Both filtered with a 121-month running mean filter for the 1893-2011 period. The unit is °C.

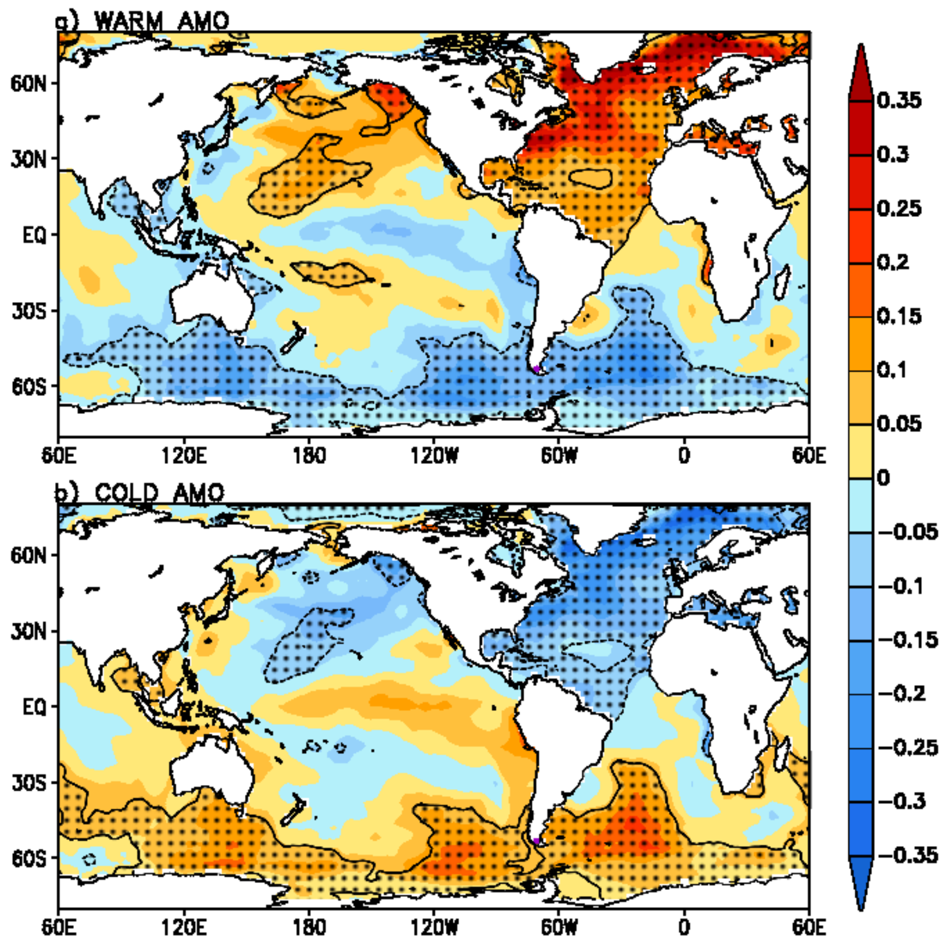

Figure 3 – SST anomalies averaged during: a) warm AMO phase; b) cold AMO phase. The unit is °C. Areas with dotted shades encompass significant values. The continuous (dashed) line encompasses positive (negative) significant anomalies at the 95% confidence level using the Student-t test for mean. The purple dot in both maps gives the location of Punta Arenas.

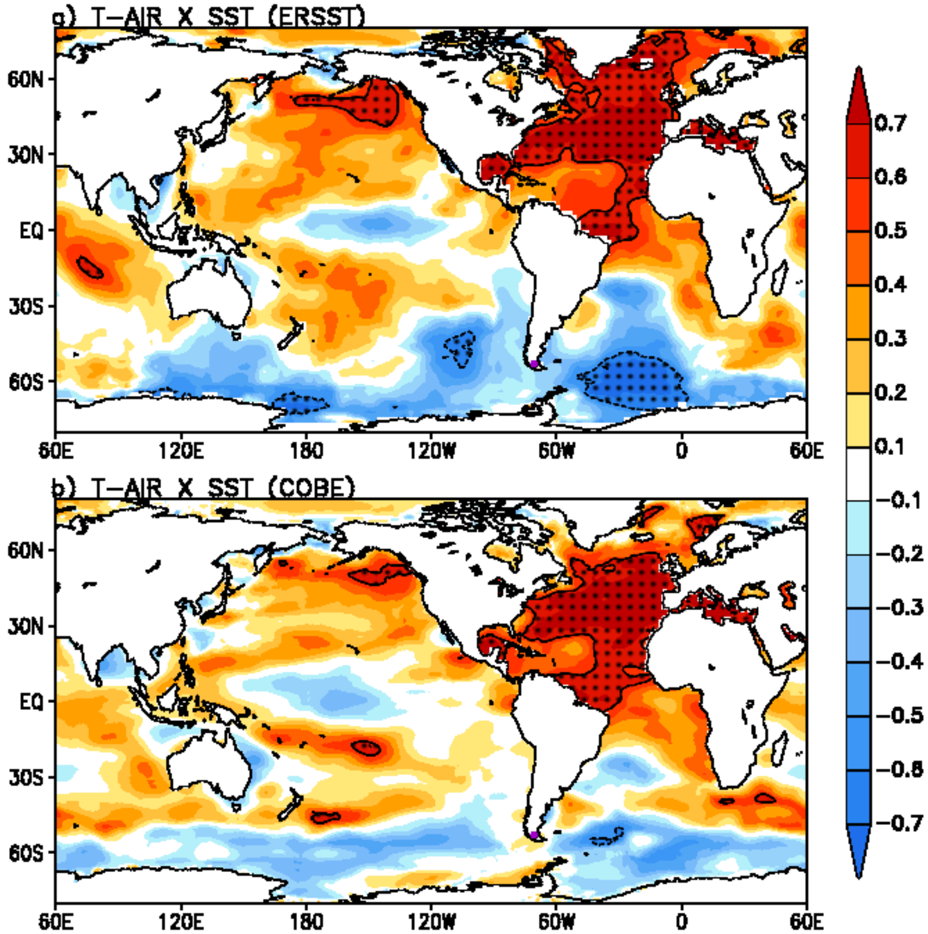

Figure 4 – Correlations between filtered PA_T-air and filtered SST using: a) ERSST data; b) COBE data. Areas with dotted shades encompass significant values. The continuous (dashed) line encompasses positive (negative) significant values at the 90% confidence level using the Ebisuzaki (1997) test for correlation. The purple dot in both maps illustrates the location of Punta Arenas.

Figure 5

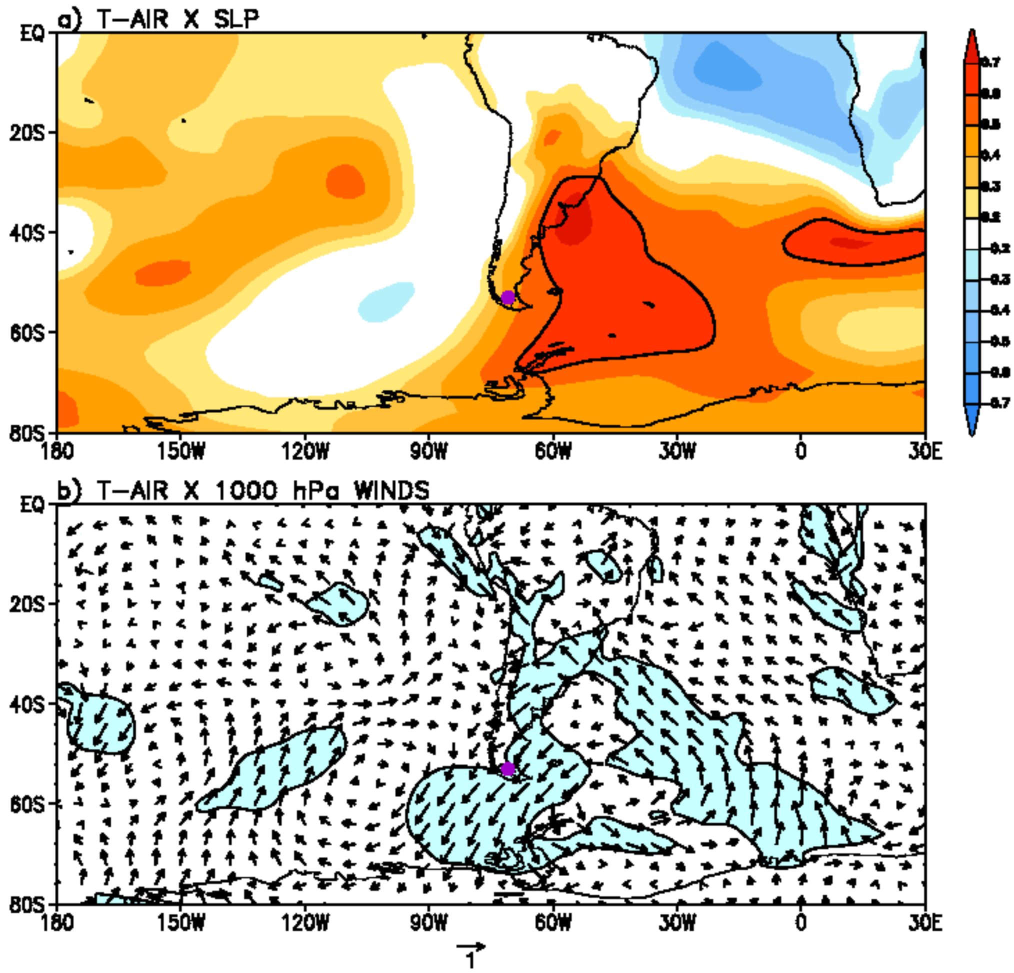

Figure 5 – Correlations between filtered PA_T-air and filtered: a) SLP; b) 1000 hPa winds. In a), the continuous (dashed) line encompasses positive (negative) significant values at the 90% confidence level using the Ebisuzaki (1997) test for correlation. In b), shaded areas encompass significant vector correlation at the 90% confidence level using the Crosby et al. (1993) test for vector correlation. Arrow at the bottom illustrates the base magnitude of the correlation vector. The purple dot in both maps illustrates the location of Punta Arenas.

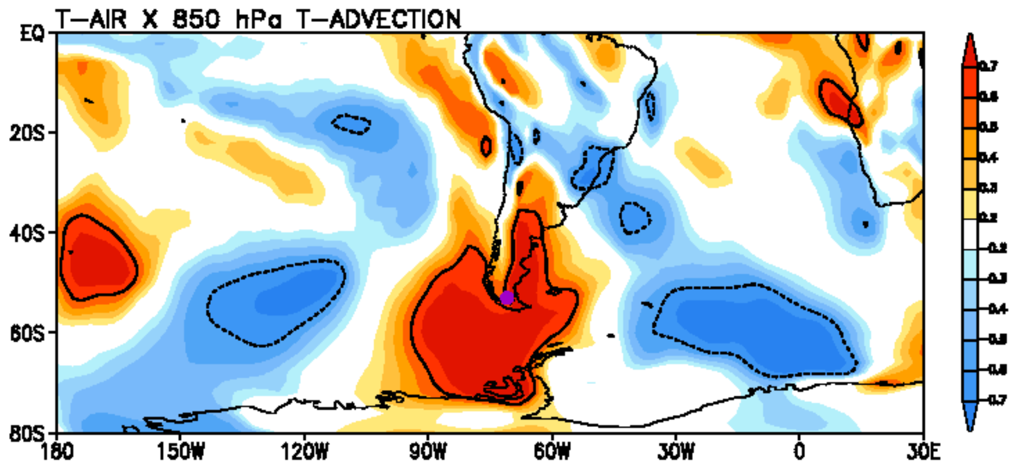

Figure 6– Correlations between filtered PA_T-air and filtered 850 hPa temperature horizontal advection. Display is the same as in Figure 5a.

Figure 7

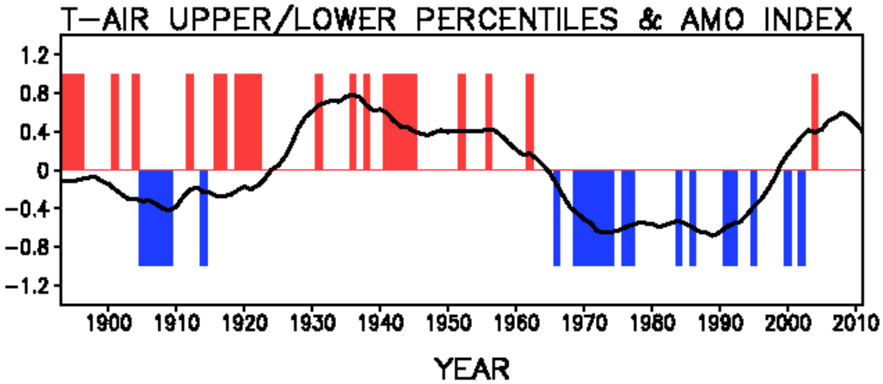

Figure 7 - Temporal occurrence of upper (blue) and lower (red) quintiles of the PA_T-air indicated, respectively by 1 and -1 and the AMO index (°C) multiplied by 3 (black continuous line).

Figure 8 Click here to download Rendered Figure Figure 8vf1.docx

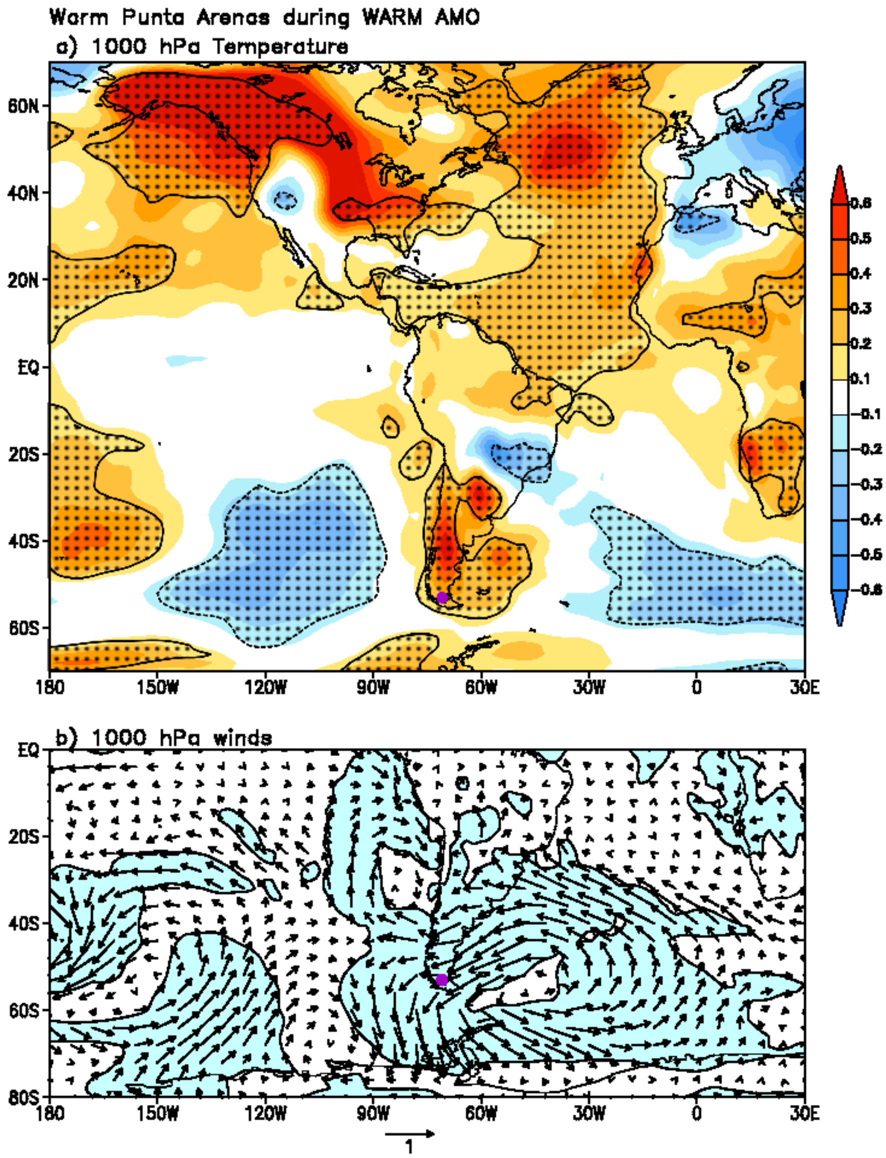

Figure 8 – a) Composites for warm Punta Arenas during the warm AMO phase of: a) 1000 hPa T-air anomalies; b) 1000 hPa wind anomalies. In a), areas with dotted shades encompass significant values and the continuous (dashed) lines encompass positive (negative) significant values. In b), shaded areas encompass significant wind vectors. The Student-t test for mean at the 90% confidence level was used. Arrow at the bottom illustrates the base magnitude of the wind vector. The units are °C for 1000 hPa T-air, and ms^{-1} for wind vector.

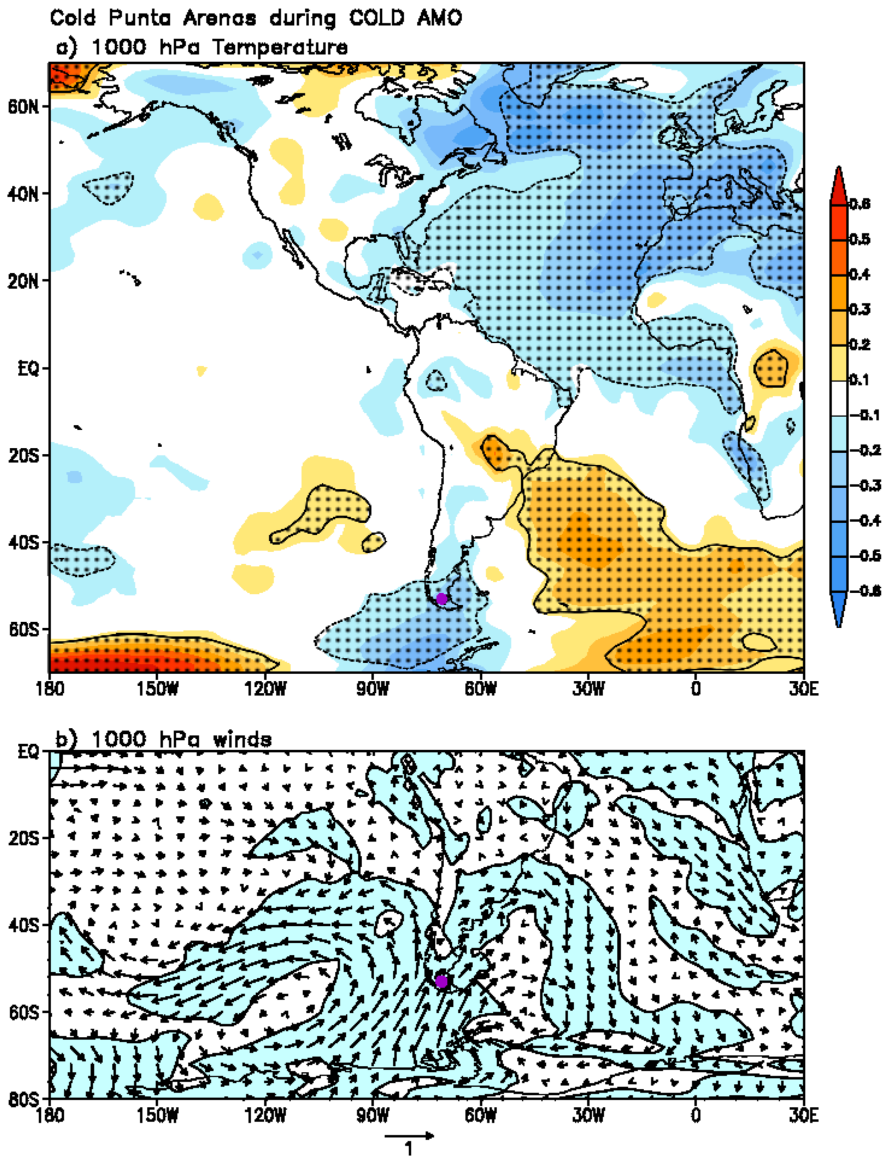

Figure 9 – a) Composites for cold Punta Arenas during the cold AMO phase of: a) 1000 hPa T-air anomalies; b) 1000 hPa wind anomalies. Display is the same as in Figure 8.